

# Dynamical fermions, centre vortices, and emergent phenomena

*Derek Leinweber<sup>1</sup>, James Biddle<sup>1</sup>, Waseem Kamleh<sup>1</sup>, and Adam Virgili<sup>1</sup>*

<sup>1</sup>Centre for the Subatomic Structure of Matter (CSSM), Department of Physics, University of Adelaide, SA, 5005, Australia

**Abstract.** The non-trivial ground-state vacuum fields of QCD form the foundation of matter. Here we examine the centre vortices identified within the ground-state fields of lattice QCD. We aim to understand the manner in which dynamical fermions in the QCD vacuum alter the centre-vortex structure. Using modern visualisation techniques, the centre-vortex structure of pure-gauge and dynamical-fermion fields is quantified and compared. We then explore the impact this modified structure has on measures of confinement and dynamical mass generation. The string tension of the static quark potential, positivity-violation in the gluon propagator, and dynamical mass generation in the overlap quark propagator are of particular interest. The impact of dynamical fermions is significant and provides new insights into the role of centre vortices in underpinning both confinement and dynamical chiral symmetry breaking in QCD.

## 1 Introduction

The essential, fundamentally-important, nonperturbative features of the QCD vacuum fields are the dynamical generation of mass through chiral symmetry breaking, and the confinement of quarks. But what is the fundamental mechanism of QCD that underpins these phenomena?

One of the most promising candidates is the centre vortex perspective of QCD vacuum structure. While the ideas of a centre-vortex dominated vacuum were laid down long ago [1–3], it wasn’t until 1997 when Jeff Greensite, Manfried Faber, *et al.* demonstrated that lattice QCD techniques could be used to explore the importance of these ideas [4–11]. Indeed by the end of the millennium, the field had attracted broad interest, with a comprehensive review in 2003 [12].

This perspective describes the nature of the nontrivial vacuum in terms of the fundamental centre of the gauge group. Herein our focus is on the SU(3) gauge group where centre vortices are characterised by the three centre phases,  $\sqrt[3]{1}$ .

By identifying centre vortices within the ground-state fields and then removing them, a deep understanding of their contributions can be developed. Removal of centre vortices from the ground-state fields results in a loss of dynamical mass generation and restoration of chiral symmetry [13–16], a loss of the string tension [17–20], a suppression of the infrared enhancement in the Landau-gauge gluon propagator [18, 21–23], and the possibility that gluons are no longer confined [23].

One can also examine the role of the centre vortices alone. Remarkably, centre vortices produce both a linear static quark potential [17, 19, 20, 24, 25] and infrared enhancement in

the Landau-gauge gluon propagator [22, 23]. The planar vortex density of centre-vortex degrees of freedom scales with the lattice spacing providing a well defined continuum limit [17]. These results elucidate strong connections between centre vortices and confinement.

A connection between centre vortices and instantons has been identified through gauge-field smoothing [25]. An understanding of the phenomena linking these degrees of freedom is illustrated in Ref. [26]. In addition, centre vortices have been shown to give rise to mass splitting in the low-lying hadron spectrum [13, 15, 27].

Still, the picture in pure SU(3) gauge theory is not perfect. The vortex-only string tension obtained from pure Yang-Mills lattice studies has been consistently shown to be about  $\sim 60\%$  of the full string tension. Moreover, upon removal of centre vortices the gluon propagator shows a remnant of infrared enhancement [22]. In short, within the pure gauge sector, the removal of long-distance non-perturbative effects via centre-vortex removal is not perfect.

Understanding the impact of dynamical fermions on the centre-vortex structure of QCD ground-state fields is a contemporary focus of the centre-vortex field [16, 19, 20, 23, 28, 29]. Herein, changes in the microscopic structure of the vortex fields associated with the inclusion of dynamical fermions are illustrated. The introduction of dynamical fermions brings the phenomenology of centre vortices much closer to a perfect encapsulation of the salient features of QCD, confinement and dynamical mass generation through chiral symmetry breaking.

As such, it is interesting to ask, what do these centre-vortex structures look like? To this end, we present visualisations of centre vortices as identified on lattice gauge-field configurations. Some of these visualisations are presented as stereoscopic images.

## 2 Centre Vortex Identification

Centre vortices are identified through a gauge fixing procedure designed to bring the lattice link variables as close as possible to the identity matrix multiplied by a phase equal to one of the three cube-roots of 1. Here, the original Monte-Carlo generated configurations are considered. They are gauge transformed directly to Maximal Centre Gauge [17, 30, 31]. This brings the lattice link variables  $U_\mu(x)$  close to the centre elements of SU(3)

$$Z = \exp\left(\frac{2\pi i}{3} n\right) \mathbf{I}, \quad (1)$$

with  $n = -1, 0, \text{ or } 1$  enumerating the three cube roots of 1 such that the special property of SU(3) matrices,  $\det(Z) = 1$ , is satisfied. One considers gauge transformations  $\mathcal{Q}$  such that,

$$\sum_{x,\mu} |\text{tr } U_\mu^{\mathcal{Q}}(x)|^2 \xrightarrow{\mathcal{Q}} \max, \quad (2)$$

and then projects the link variables to the centre

$$U_\mu(x) \rightarrow Z_\mu(x) \text{ where } Z_\mu(x) = \exp\left(\frac{2\pi i}{3} n_\mu(x)\right) \mathbf{I}. \quad (3)$$

Here,  $n$  has been promoted to a field,  $n_\mu(x)$ , taking a value of  $-1, 0, \text{ or } 1$  for each link variable on the lattice. In this way, the gluon field,  $U_\mu(x)$ , is characterised by the most fundamental aspect of the SU(3) link variable, the centre,  $Z_\mu(x)$ . In the projection step, eight degrees of freedom are reduced to one of the three centre phases. This “vortex-only” field,  $Z_\mu(x)$ , can be examined to learn the extent to which centre vortices alone capture the essence of nonperturbative QCD.

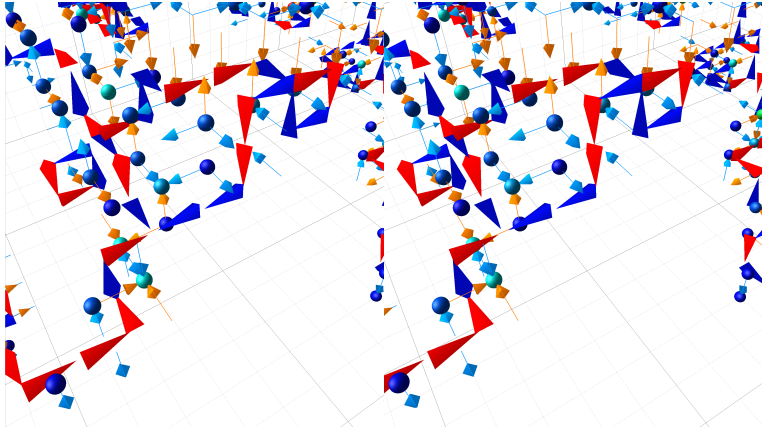


**Figure 1.** Stereoscopic image of centre vortices as identified on the lattice from Ref. [28]. Vortex features including vortex lines (jets), branching points (3-jet combinations), crossing points (4 jets), indicator links (arrows) and singular points (spheres) are described in the text.

The product of these centre-projected links,  $Z_\mu(x)$ , around an elementary  $1 \times 1$  square (plaquette) on the lattice also produces a centre element of SU(3). The value describes the centre charge associated with that plaquette

$$z = \prod_{\square} Z_\mu(x) = \exp\left(2\pi i \frac{m}{3}\right), \quad m = -1, 0, \text{ or } 1. \quad (4)$$

The most common value observed has  $m = 0$  indicating that no centre charge pierces the plaquette. However, values of  $m = \pm 1$  indicate that the centre line of an extended three-dimensional vortex pierces that plaquette.

The complete centre-line of an extended vortex is identified by tracing the presence of nontrivial centre charge,  $m = \pm 1$ , through the spatial lattice. Figure 1 exhibits rich emergent structure in the nonperturbative QCD ground-state fields in a stereoscopic image. Here a 3D slice of the 4D space-time lattice is being considered at fixed time. To experience figure 1 in 3D, try the following:

1. If you are viewing the image on a monitor, ensure the image width is 12 to 13 cm.
2. Bring your eyes very close to one of the image pairs.
3. Close your eyes and relax.
4. Open your eyes and allow the (blurry) images to line up. Tilting your head from side to side will move the images vertically.
5. Move back slowly until your eyes are able to focus. There's no need to cross your eyes!

Features of the vortex phenomena include:

#### Vortex Lines:

The plaquettes with nontrivial centre charge, characterised by  $m = +1$  or  $-1$ , are plotted as jets piercing the centre of the plaquette. Both the orientation and colour of the jets reflect the value of the non-trivial centre charge. Using a right-hand rule for the direction, plaquettes with  $m = +1$  are illustrated by blue jets in the forward direction, and plaquettes with  $m = -1$  are illustrated by red jets in the backward direction. Thus, the jets show the directed flow of

$m = +1$  centre charge,  $z = e^{2\pi i/3}$ , through spatial plaquettes. They are analogous to the line running down the centre of a vortex in a fluid.

Vortices are somewhat correlated with the positions of significant topological charge density, but not in a strong manner [26]. However, the percolation of vortex structure is significant and the removal of these vortices destroys most instanton-like objects.

#### *Branching Points or Monopoles:*

In SU(3) gauge theory, three vortex lines can merge into or emerge from a single point. Their prevalence is surprising, as is their correlation with topological charge density [26].

#### *Vortex Sheet Indicator Links:*

As the vortex line moves through time, it creates a vortex sheet in 4D spacetime. This movement is illustrated by arrows along the links of the lattice (shown as cyan and orange arrows in figure 1) indicating centre charge flowing through space-time plaquettes in the suppressed time direction.

#### *Singular Points:*

When the vortex sheet spans all four space-time dimensions, it can generate topological charge. Lattice sites with this property are called singular points [9, 32–34] and are illustrated by spheres. The sphere colour indicates the number of times the sheet adjacent to a point can generate a topological charge contribution [26].

## 3 Impact of Dynamical Fermions

First results demonstrating the impact of dynamical fermions on the centre-vortex structure of QCD ground-state fields were presented in Ref. [29]. Here we introduce improved visualisation algorithms and explore alternative time slices.

Matched lattices are considered, one in pure-gauge and the other a 2 + 1-flavor dynamical-fermion lattice from the PACS-CS Collaboration [35]. These  $32^3 \times 64$  lattice ensembles employ a renormalisation-group improved Iwasaki gauge action and non-perturbatively  $O(a)$ -improved Wilson quarks, with  $C_{SW} = 1.715$ .

The lightest  $u$ - and  $d$ -quark-mass ensemble identified by a pion mass of 156 MeV [35] is presented here. The scale is set using the Sommer parameter with  $r_0 = 0.4921$  fm providing a lattice spacing of  $a = 0.0933$  fm [35]. A matched  $32^3 \times 64$  pure-gauge ensemble using the same improved Iwasaki gauge action with a Sommer-scale spacing of  $a = 0.100$  fm is created to enable comparisons with the PACS-CS ensembles.

The centre-vortex structure of pure-gauge and dynamical-fermion ground-state vacuum fields is illustrated in figures 2 and 3 respectively. These are interactive plots which can be activated by clicking on the image in Adobe Reader<sup>1</sup>. Once activated, click and drag to rotate, Ctrl-click to translate, Shift-click or mouse wheel to zoom, and right click to access the “Views” menu. Several views identifying interesting features have been created to facilitate an inspection of the centre-vortex structure.

In both illustrations, the vortex structure is dominated by a single large percolating structure, a characteristic feature of the confining phase [36]. Whereas small loops will tend to

---

<sup>1</sup>To interact with these models, it is necessary to open this document in Adobe Reader or Adobe Acrobat (requires version 9 or newer). Linux users may install Adobe Acroread version 9.4.1 (the last edition to have full 3D support), or use a Windows emulator such as PlayOnLinux. From the Adobe “Edit” menu, select “Preferences...” and ensure “3D & Multimedia” is enabled and “Enable double-sided rendering” is selected.

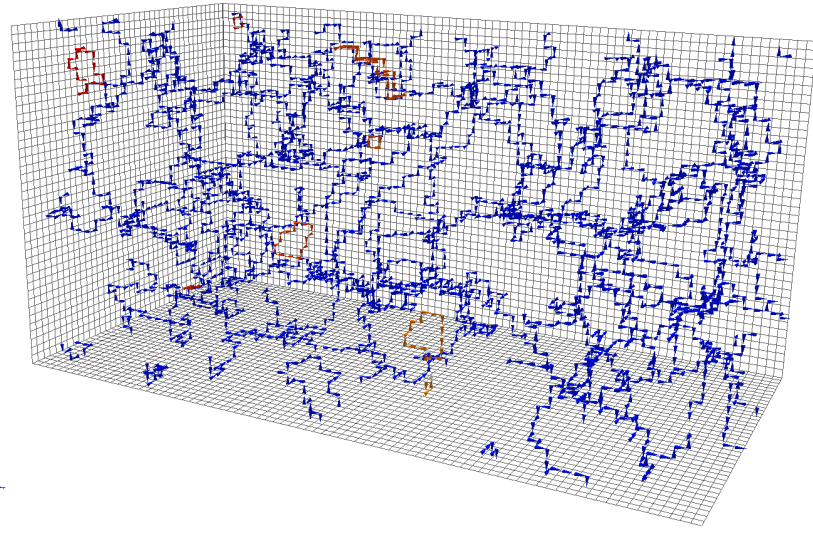


**Figure 2.** The centre vortex structure of a ground-state vacuum field configuration in pure SU(3) gauge theory. The flow of +1 centre charge through the gauge field is illustrated by the jets (see main text for a description of the plotting conventions). Here, blue jets are used to illustrate the primary percolating vortex cluster, while other colours illustrate the secondary clusters. (*Click to activate.*)

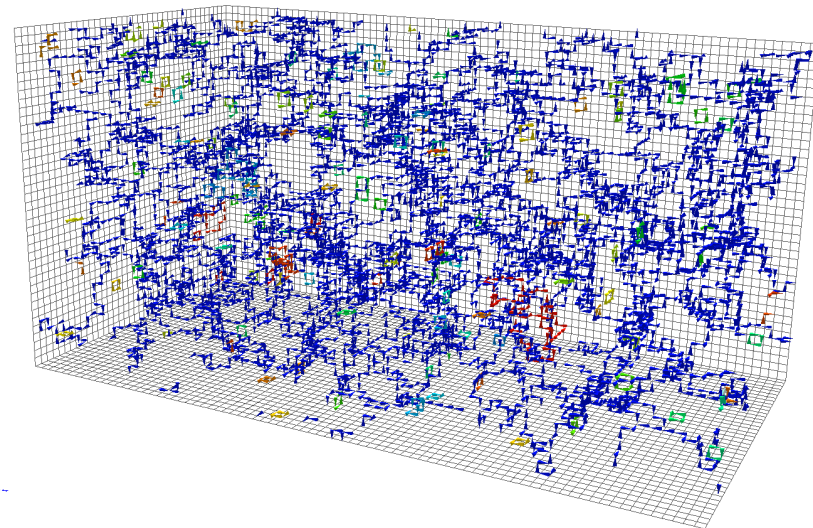


**Figure 3.** The centre-vortex structure of a ground-state vacuum field configuration in dynamical 2+1 flavour QCD with  $m_\pi = 156$  MeV. Symbols are as described in figure 2. (*Click to activate.*)

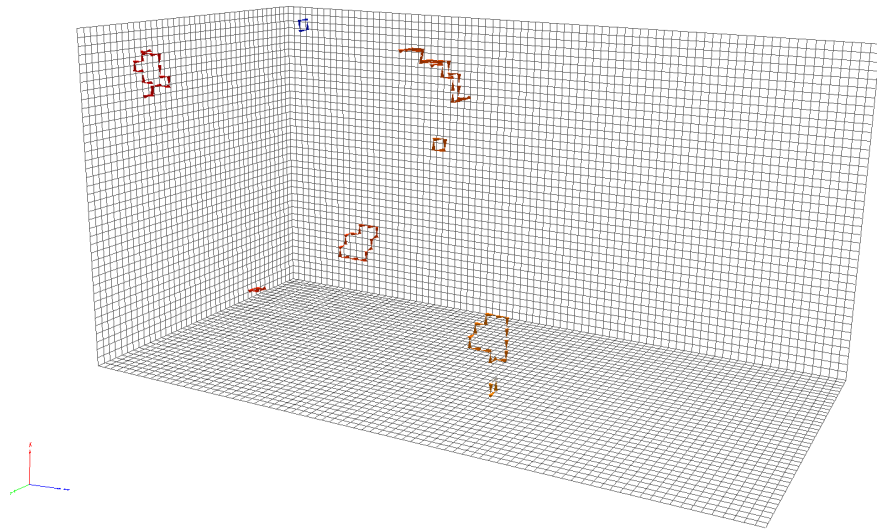


**Figure 4.** The centre-vortex structure of the secondary loops identified from the pure-gauge configuration shown in figure 2. (*Click to activate.*)

---

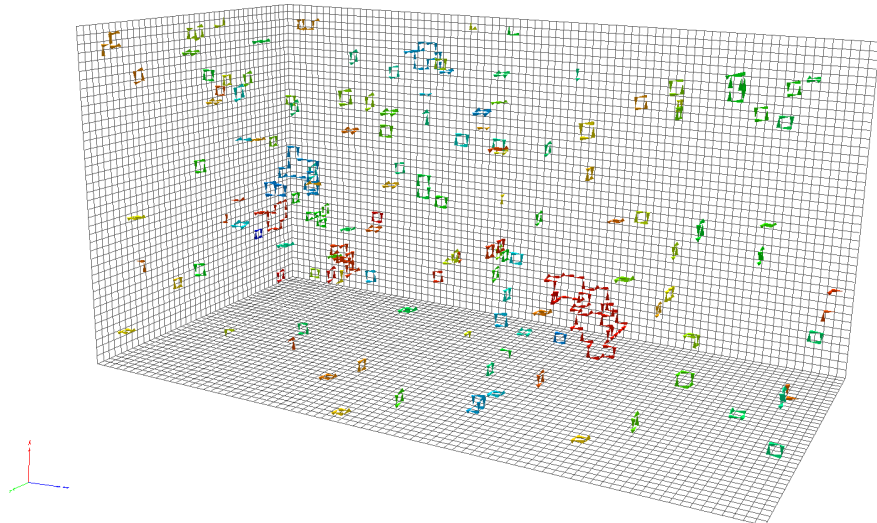


**Figure 5.** The centre-vortex structure of the secondary loops identified from the dynamical-fermion configuration shown in figure 3. (*Click to activate.*)

pierce a Wilson loop twice with zero effect, it is this extended structure that gives rise to a net vortex piercing of a Wilson loop and the generation of an area law associated with confinement. These two illustrations are representative of the ensemble in that the vortex structure is typically dominated by a single large percolating cluster.

Closer inspection reveals a continuous flow of centre charge, often emerging or converging to monopole or anti-monopole vertices where three jets emerge from or converge to a point. These are also referred to as branching points [37], as a +1 centre charge flowing out of a vertex is equivalent to +2 centre charge flowing into the vertex and subsequently branching to two +1 jets flowing out of the vertex.

Figures 4 and 5 illustrate the same time slices as in figures 2 and 3 but with the primary percolating clusters removed. The vortex structure of the secondary clusters in the dynamical-fermion case is more complex, typically featuring branching points in their structure. Again, views have been created in the interactive figures to identify interesting features and link their locations between the full and secondary structure illustrations.

With the introduction of dynamical fermions, the structure becomes more complex, both in the abundance of vortices and branching points. The average number of vortices composing the primary cluster in these  $32^2 \times 64$  spatial slices roughly doubles from  $\sim 3,000$  vortices in the pure gauge theory to  $\sim 6,000$  in full QCD. Still, there are  $32^2 \times 64 \times 3 = 196,608$  spatial plaquettes on these lattices and thus the presence of a vortex is a relatively rare occurrence.

By counting the number of vortices between branching points one discovers the distribution is exponential, indicating a constant branching probability. This probability is higher in full QCD by a ratio of  $\sim 3/2$ .

## 4 Static Quark Potential

With an understanding of the impact of dynamical-fermion degrees of freedom on the centre-vortex structure of ground-state vacuum fields, attention has turned to understanding the impact on confinement. In a variational analysis of standard Wilson loops composed of several spatially-smeared sources to isolate the ground state potential, the static quark potential has been calculated on three ensembles including the original untouched links,  $U_\mu(x)$ , the vortex-only links,  $Z_\mu(x)$ , and vortex-removed links,  $Z_\mu^\dagger(x) U_\mu(x)$  [23] where the multiplication of the conjugate of the centre-projected field ensure all plaquettes have  $z = 0$ .

For the original untouched configurations, the static quark potential is expected to follow a Cornell potential

$$V(r) = V_0 - \frac{\alpha}{r} + \sigma r. \quad (5)$$

As centre vortices are anticipated to encapsulate the non-perturbative long-range physics, the vortex-only results should give rise to a linearly rising potential. On the other hand, the vortex-removed results are expected to capture the short-range Coulomb behaviour. Figure 6 from Ref. [23] illustrates the static quark potentials obtained from these three ensembles for the pure-gauge and dynamical 2 + 1-flavor ensemble with a pion mass of 156 MeV [35].

Qualitatively, centre vortices account for the long-distance physics. The removal of centre vortices completely removes the confinement potential. And while the vortex-only string tension is typically 60 % of the original string tension in the pure gauge sector, the introduction of dynamical fermions has improved the vortex-only phenomenology significantly. Vortices alone capture both the screening of the pure-gauge string tension and the full string tension of the original untouched ensemble. This result is associated with the significant modification of the centre-vortex structure of ground-state vacuum fields induced by dynamical fermions.

The vortex-removed potential enables an examination of the Coulomb term in the ansatz of Eq. (5) and its ability to characterise the short-distance aspects of QCD in the absence

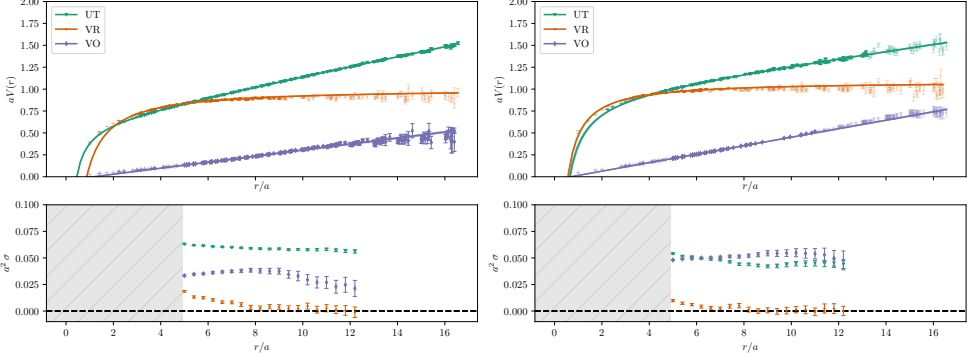


**Figure 6.** The static quark potential calculated on the vortex-modified pure-gauge (left) and  $m_\pi = 156$  MeV dynamical-fermion (right) ensembles. The lower plot shows the local slope from linear fits of the potentials in the upper plot over a forward-looking window from  $r$  to  $r + 4a$ .

of confinement. We find the long-range aspect of the Coulomb term to be inconsistent with the vortex-removed potential. This is illustrated in figure 6 by fading out the lattice QCD results that are inconsistent with the Coulomb ansatz. Potentials including (anti-)screening considerations to capture the correct physics are recommended in Ref. [19]. Indeed, the standard extraction of the string tension is spoiled by the persistent nature of the Coulomb term and alternative forms are discussed in detail [19].

## 5 Gluon propagator and positivity violation

The improved separation of perturbative and nonperturbative physics through the consideration of vortex-removed and vortex-only ensembles in full QCD is also manifest in the nonperturbative gluon propagator [23]. This time vortex removal removes the infrared enhancement of the gluon propagator, leaving a tree-level like structure as illustrated in figure 7 for the gluon-propagator renormalisation function  $Z(q^2) = q^2 D(q^2)$ . Of course, finite-volume effects force  $Z(q^2) \rightarrow 0$  as  $q^2 \rightarrow 0$  as  $D(q^2)$  is finite. Details of the renormalisation procedure are summarised at the end of Sec. III A in Ref. [23].

To explore positivity violation, one considers the Euclidean correlator,  $C(t)$ , obtained by taking the Fourier transform of  $D(q_0, \mathbf{0})$  such that [23]

$$C(t) = \frac{1}{2\pi} \int_{-\infty}^{\infty} dq_0 \int_0^{\infty} dm^2 \frac{\rho(m^2)}{q_0^2 + m^2} e^{-iq_0 t}. \quad (6)$$

Extending the  $q_0$  integral to the complex plane and employing the residue theorem, one arrives at

$$C(t) = \int_0^{\infty} dm e^{-mt} \rho(m^2). \quad (7)$$

Clearly if  $C(t) < 0$  for any  $t$  then  $\rho(m^2)$  is not positive definite, and we say that positivity has been violated. This implies that there is no Källen-Lehmann representation and as such the propagator does not represent a correlation between physical states. Hence, the states do not appear in the physical spectrum. In the context of the gluon propagator, this can be taken as an indication that gluons are confined.

The numerical calculation of Eq. (7) is described in detail in Ref. [23], where the subtleties of the finite volume are fully accounted for. The results are shown in figure 8. As

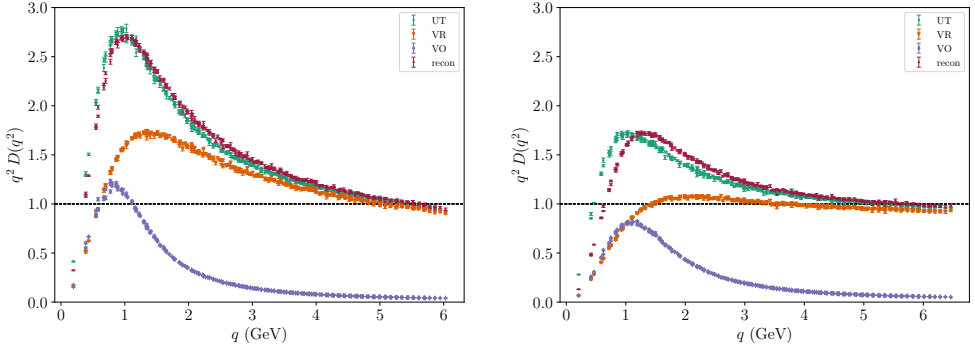


**Figure 7.** The pure-gauge gluon propagator (left) is compared with the  $m_\pi = 156$  MeV dynamical-fermion gluon propagator (right). The propagators are renormalised as described in the text. UT refers to the original untouched configurations, VR to the vortex-removed configurations and VO to the vortex-only configurations. The “recon” results are a reconstruction of the original propagator obtained from a linear combination of the vortex-only and vortex-removed propagators.

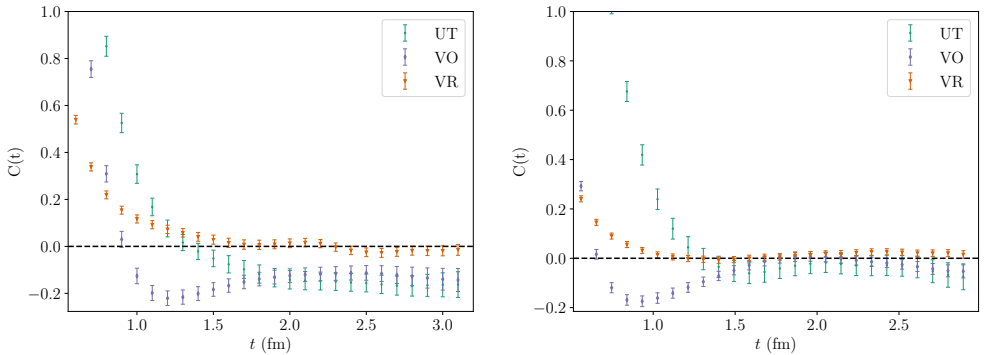


**Figure 8.** The pure-gauge Euclidean correlator (left) is compared with the  $m_\pi = 156$  MeV dynamical-fermion Euclidean correlator (right). Shown are the results from the untouched (UT), vortex-removed (VR) and vortex-only (VO) ensembles. A dashed line at  $C(t) = 0$  is provided to aid in observing positivity violation.

expected [38], the untouched correlator shows clear signs of positivity violation. Interestingly, the vortex-only correlators also exhibit robust positivity violation.

The positivity violation present in the pure-gauge vortex-removed result at large distances is consistent with the observations made in figure 7, where residual infrared strength in the vortex-removed gluon propagator is apparent. Thus, the separation of perturbative and non-perturbative physics through vortex modification is imperfect in the pure-gauge sector.

The results from the dynamical ensemble in the right-hand plot of figure 8 demonstrate an interesting change in behaviour. As with the gluon propagator results in the previous section, the most striking change is in the vortex-removed correlator. In this sector we now observe consistency with positivity in the dynamical-fermion case. This supports the interpretation of the positivity violation in the vortex-removed pure-gauge results as being related to the residual non-perturbative infrared strength in the gluon propagator. As this residual strength is significantly diminished on the dynamical ensembles, we now see that the residual  $q^2$

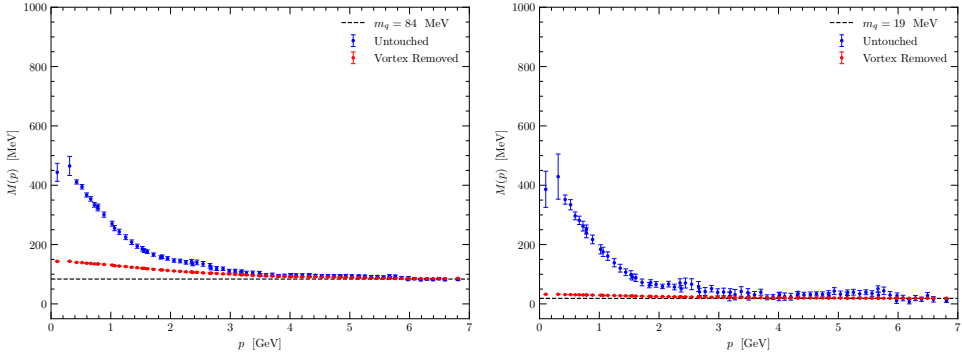


**Figure 9.** The mass functions,  $M(p)$ , on untouched and vortex-removed dynamical-fermion ensembles for valence-quark masses  $m_q = 84$  MeV (left), and  $m_q = 19$  MeV (right). Explicit chiral symmetry breaking through the quark mass leaves a remnant of dynamical mass generation.

dependence in the VR renormalisation function may be purely perturbative in origin. In this case, vortex modification has been successful in separating perturbative and non-perturbative physics.

In summary, the vortex-only ensembles capture the infrared enhancement of the gluon propagator and the screening of this enhancement in full QCD. Moreover, the vortex-only configurations exhibit significant positivity violation, as would be expected of a confining infrared-dominated theory. Conversely, the vortex-removed dynamical-fermion configurations show a loss of this positivity violation, admitting the possibility that they do support a spectral representation of the propagator constructed from perturbative gluon interactions. These results provide additional support for the fact that centre vortices encapsulate the confining aspects of QCD.

## 6 Quark propagator and dynamical mass generation

The overlap Landau-gauge quark propagator  $S(p)$  can be written in the form

$$S(p) = \frac{Z(p)}{iq + M(p)}, \quad (8)$$

where  $Z(p)$  is the renormalisation function and  $M(p)$  is the mass function, and  $q$  is a tree-level improved momentum variable minimising lattice artefacts [39]. The infrared behaviour of the mass function, specifically, the presence of dynamical mass generation, provides a clear signal of dynamical chiral symmetry breaking.

Figure 9 compares the  $q^2$ -dependent overlap-Dirac quark-propagator Landau-gauge mass function on the light dynamical-fermion ensemble for two different valence-quark masses. In comparison to the pure-gauge sector dynamical mass generation is suppressed under vortex removal in full QCD [16].

While explicit chiral symmetry breaking through the quark mass leaves a remnant of dynamical mass generation, it is anticipated that for sufficiently light current quark masses, chiral symmetry will be restored [15] and dynamical mass generation will be completely eliminated in the vortex-removed theory.

## 7 Summary

In summary, centre-vortex structure is complex. Each ground-state configuration is dominated by a long-distance percolating centre-vortex structure. In SU(3) gauge field theory, a proliferation of branching points is observed, with further enhancement as light dynamical fermion degrees of freedom are introduced in simulating QCD. There is an approximate doubling in the number of nontrivial centre charges in the percolating vortex structure as one goes from the pure-gauge theory to full QCD. Increased complexity in the vortex paths is also observed as the number of branching points is significantly increased with the introduction of dynamical fermions. In short, dynamical-fermion degrees of freedom radically alter the centre-vortex structure of the ground-state vacuum fields. This change in structure acts to improve the phenomenology of centre vortices better reproducing the string tension, dynamical mass generation and better removing nonperturbative physics under vortex removal. This represents a significant advance in the ability of centre vortices to capture the salient nonperturbative features of QCD.

## Acknowledgements

DBL thanks Jeff Greensite for several interesting conversations on centre vortices during the conference. We thank the PACS-CS Collaboration for making their 2 + 1 flavour configurations available via the International Lattice Data Grid (ILDG). This research was undertaken with the assistance of resources from the National Computational Infrastructure (NCI), provided through the National Computational Merit Allocation Scheme and supported by the Australian Government through Grant No. LE190100021 via the University of Adelaide Partner Share. This research is supported by Australian Research Council through Grants No. DP190102215 and DP210103706. WK is supported by the Pawsey Supercomputing Centre through the Pawsey Centre for Extreme Scale Readiness (PaCER) program.

## References

- [1] G. 't Hooft, Nucl. Phys. B **138**, 1 (1978)
- [2] G. 't Hooft, Nucl. Phys. B **153**, 141 (1979)
- [3] H.B. Nielsen, P. Olesen, Nucl. Phys. B **160**, 380 (1979)
- [4] L. Del Debbio, M. Faber, J. Greensite, S. Olejnik, Phys. Rev. D **55**, 2298 (1997), [hep-lat/9610005](#)
- [5] M. Faber, J. Greensite, S. Olejnik, Phys. Rev. D **57**, 2603 (1998), [hep-lat/9710039](#)
- [6] L. Del Debbio, M. Faber, J. Giedt, J. Greensite, S. Olejnik, Phys. Rev. D **58**, 094501 (1998), [hep-lat/9801027](#)
- [7] R. Bertle, M. Faber, J. Greensite, S. Olejnik, JHEP **03**, 019 (1999), [hep-lat/9903023](#)
- [8] M. Faber, J. Greensite, S. Olejnik, D. Yamada, JHEP **12**, 012 (1999), [hep-lat/9910033](#)
- [9] M. Engelhardt, H. Reinhardt, Nucl. Phys. B **567**, 249 (2000), [hep-th/9907139](#)
- [10] R. Bertle, M. Faber, J. Greensite, S. Olejnik, JHEP **10**, 007 (2000), [hep-lat/0007043](#)
- [11] M. Engelhardt, M. Quandt, H. Reinhardt, Nucl. Phys. B **685**, 227 (2004), [hep-lat/0311029](#)
- [12] J. Greensite, Prog. Part. Nucl. Phys. **51**, 1 (2003), [hep-lat/0301023](#)
- [13] A. Trewartha, W. Kamleh, D. Leinweber, Phys. Lett. **B747**, 373 (2015), [1502.06753](#)
- [14] J. Greensite, EPJ Web Conf. **137**, 01009 (2017), [1610.06221](#)
- [15] A. Trewartha, W. Kamleh, D. Leinweber, J. Phys. **G44**, 125002 (2017), [1708.06789](#)

- [16] A. Virgili, W. Kamleh, D. Leinweber, PoS **LATTICE2021**, 082 (2021), [2204.06978](#)
- [17] K. Langfeld, Phys. Rev. **D69**, 014503 (2004), [hep-lat/0307030](#)
- [18] P.O. Bowman, K. Langfeld, D.B. Leinweber, A. Sternbeck, L. von Smekal, A.G. Williams, Phys. Rev. D **84**, 034501 (2011), [1010.4624](#)
- [19] J.C. Biddle, W. Kamleh, D.B. Leinweber, Phys. Rev. D **106**, 054505 (2022), [2206.00844](#)
- [20] D. Leinweber, J. Biddle, W. Kamleh, SciPost Phys. Proc. **6**, 004 (2022), [2205.12518](#)
- [21] K. Langfeld, H. Reinhardt, J. Gattnar, Nucl. Phys. B **621**, 131 (2002), [hep-ph/0107141](#)
- [22] J.C. Biddle, W. Kamleh, D.B. Leinweber, Phys. Rev. **D98**, 094504 (2018), [1806.04305](#)
- [23] J.C. Biddle, W. Kamleh, D.B. Leinweber, Phys. Rev. D **106**, 014506 (2022), [2206.02320](#)
- [24] A. O'Cais, W. Kamleh, K. Langfeld, B. Lasscock, D. Leinweber, P. Moran, A. Sternbeck, L. von Smekal, Phys. Rev. D **82**, 114512 (2010), [0807.0264](#)
- [25] A. Trewartha, W. Kamleh, D. Leinweber, Phys. Rev. **D92**, 074507 (2015), [1509.05518](#)
- [26] J.C. Biddle, W. Kamleh, D.B. Leinweber, Phys. Rev. D **102**, 034504 (2020), [1912.09531](#)
- [27] E.A. O'Malley, W. Kamleh, D. Leinweber, P. Moran, Phys. Rev. D **86**, 054503 (2012), [1112.2490](#)
- [28] J.C. Biddle, W. Kamleh, D.B. Leinweber, EPJ Web Conf. **245**, 06009 (2020), [2009.12044](#)
- [29] D. Leinweber, J. Biddle, W. Kamleh, PoS **LATTICE2021**, 197 (2021), [2204.04825](#)
- [30] L. Del Debbio, M. Faber, J. Greensite, S. Olejnik, Phys. Rev. **D55**, 2298 (1997), [hep-lat/9610005](#)
- [31] K. Langfeld, H. Reinhardt, O. Tennert, Phys. Lett. **B419**, 317 (1998), [hep-lat/9710068](#)
- [32] F. Bruckmann, M. Engelhardt, Phys. Rev. **D68**, 105011 (2003), [hep-th/0307219](#)
- [33] M. Engelhardt, Phys. Rev. **D83**, 025015 (2011), [1008.4953](#)
- [34] M. Engelhardt, Nucl. Phys. **B585**, 614 (2000), [hep-lat/0004013](#)
- [35] S. Aoki et al. (PACS-CS), Phys. Rev. D **79**, 034503 (2009), [0807.1661](#)
- [36] M. Engelhardt, K. Langfeld, H. Reinhardt, O. Tennert, Phys. Rev. D **61**, 054504 (2000), [hep-lat/9904004](#)
- [37] F. Spengler, M. Quandt, H. Reinhardt, Phys. Rev. **D98**, 094508 (2018), [1810.04072](#)
- [38] P.O. Bowman, U.M. Heller, D.B. Leinweber, M.B. Parappilly, A. Sternbeck, L. von Smekal, A.G. Williams, J.b. Zhang, Phys. Rev. D **76**, 094505 (2007), [hep-lat/0703022](#)
- [39] A. Virgili, W. Kamleh, D. Leinweber (2022), [2209.14864](#)